COMPUTER-BASED FACTORY AUTOMATION

11th Conference on Production Research & Technology

Conference Proceedings

May 21-23, 1984

COMPUTER-BASED FACTORY AUTOMATION

11th Conference on Production Research and Technology

Conference Proceedings

May 21-23, 1984
Carnegie-Mellon University
Pittsburgh, Pennsylvania

Sponsored by
National Science Foundation
Production Research Program
Washington, D.C. 20550

Published by
Society of Manufacturing Engineers
One SME Drive
P.O. Box 930
Dearborn, Michigan 48121

PROCEEDINGS

COMPUTER-BASED FACTORY AUTOMATION

First Edition
First Printing

Library of Congress Catalog Number: 84-50766
International Standard Book Number: 0-87263-149-4
Manufactured in the United States of America

PREFACE

These Proceedings contain the presentations from the Eleventh Conference on Production Research and Technology. The papers have been prepared by the grant-recipients of the National Science Foundation's program in Production Research and Technology, concerned with Computer Based Factory Automation.

It is hoped that these research reports are of particular interest to production engineers, research managers and university faculty engaged in advanced automation and manufacturing.

In this proceedings' volume, the papers will have been grouped into the four main areas of: i) process-physics, ii) controls and robotics, iii) design for manufacturing, and iv) information and the management of manufacturing. These arbitrary divisions form a framework for structuring (reminiscent of Bohr's atom) this multidisciplinary research area of Manufacturing Engineering:

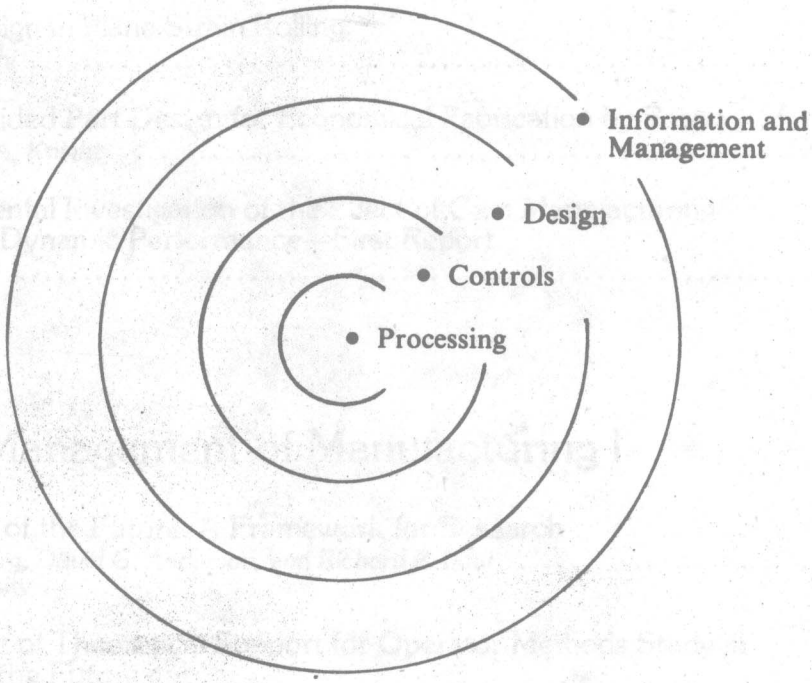

It has been a privilege to work with Dr. Bill Spurgeon of the National Science Foundation and to host this 1984 Conference at Carnegie-Mellon University in Pittsburgh. The Society of Manufacturing Engineers is thanked for its cooperation in producing this bound volume. Particular thanks go to Tanya Rogers who has served as the Conference secretary and administrator.

Paul K. Wright
Mechanical Engineering Dept.
and the Robotics Institute
Carnegie-Mellon University
Pittsburgh, PA 15213

TABLE OF CONTENTS

Part I: Design for Manufacturing I

Part II: Management of Manufacturing I

Part III: Manufacturing Process-Physics I

Part IV: Controls and Robotics I

Part V: Management of Manufacturing II

Part VI: Manufacturing Process-Physics II

Part VII: Controls and Robotics II

Part VIII: Design for Manufacturing II

Part IX: Manufacturing Process-Physics III

Part X: Controls and Robotics III

Part I

Design for Manufacturing I

Part I

Design for Manufacturing I

Computer Applications in Injection Molding

K.K. Wang
Sibley School of Mechanical and Aerospace Engineering
Cornell University

C.A. Hieber
Sibley School of Mechanical and Aerospace Engineering
Cornell University

S.F. Shen
Sibley School of Mechanical and Aerospace Engineering
Cornell University

C. Cohen
School of Chemical Engineering
Cornell University

A.I. Isayev
Sibley School of Mechanical and Aerospace Engineering
Cornell University

ABSTRACT. This paper summarizes results obtained by the Cornell Injection Molding Program during the past funding period, as documented in Progress Report No. 10 which was released in January 1984. In particular, further injection-molding experiments have shown good agreement with inelastic predictions for cavity pressure during filling and have enabled deducing juncture gate losses. The latter have been found to be decidedly smaller for polycarbonate than for polystyrene or polypropylene and to increase with glass-fiber-filler content. Frozen-in density distributions in injection-molded polystyrene have been measured by means of a density-gradient column and found to be most sensitive to packing pressure and injection melt temperature; such density variations, however, have been on the order of only a tenth of one percent. Corresponding part-weight measurements have indicated variations on the order of a few percent which have correlated well with shrinkage measurements. Progress has been made in developing an interactive package for "laying a part flat" and a color-coded graphics package for displaying calculated temperature and pressure distributions in the cavity. An investigation has been made into the non-isothermal flow of polymeric melts in cold-wall non-circular runners and work has continued with measuring flow birefringence in converging and diverging channels. Frozen-in birefringence measurements in molded polystyrene strips have shown the appearance of two local peaks across the half gap in the end closest to the gate, the second peak apparently arising from the flow during the packing stage. Work has continued with developing a unified constitutive equation and with successfully applying the Leonov model to one-dimensional elongational flow under transient non-isothermal flow. Studies with glass-fiber-filled polymers have indicated a systematic decrease in shear viscosity upon being extruded or injection molded; the frozen-in glass-fiber orientation in injection-molded parts has been documented by detailed plots of reflect-type microscopic observations. Process-control studies have been initiated in developing a method for obtaining parameter estimates for a dynamic system in which injection velocity is the controlled variable. A program has been developed for simulating NC mold machining with application to the milling operation; a shaded display of the simulated part as well as the swept volume of the tool can be generated on a color-raster graphic terminal. Work has also proceeded with developing a technique for NC data generation and display and with developing a two-dimensional finite-element mesh generator for the TIPS-1 system.

PRESSURE LOSSES IN JUNCTURE FLOW REGIONS. In general, flow simulations of the filling stage in injection molding have relied upon inelastic, shear-flow-dominated models which neglect any juncture losses which may occur in the runner system (due to 90° turns, e.g.), in the gate region (due to abrupt changes in flow area) or in the cavity itself (due to possible bends in the part, e.g., which would be neglected upon "laying the part flat"). As one means of addressing this problem area, we have performed a series of experiments with various polymeric melts in a heavily instrumented mold; by comparing the measured experimental traces with corresponding inelastic predictions, it is possible to deduce the level of the neglected juncture losses. This is illustrated by Fig. 1 which shows representative experimental (curves) and predicted (symbols) pressure traces at five locations in the system for a specific set of flow conditions with polypropylene. In particular, the first three traces correspond to transducer locations along the runner whereas transducers 4 and 5 lie within the cavity. It is noted that the abrupt rise in traces 1-3 at $t \simeq .65$ sec corresponds to when the melt reaches the highly resistive, small gate region. Whereas the predictions model traces 1-3 quite well before this point, it is noted that the symbols lie systematically below curves 1-3 once the melt reaches the gate. The point to be noted, however, is that the latter discrepancy is fairly constant and almost the same ($\simeq$ 400 psi) in all three cases. On the other hand, the corresponding predictions for the cavity pressure traces, 4 and 5, are seen to be very good. Accordingly, the above discrepancy in traces 1-3 can be attributed to a juncture loss at the gate. Further results in this regard are shown in Figs. 2 and 3. In particular, ΔP_{4-5} in the former figure denotes the cavity pressure drop between transducers 4 and 5 at the instant the melt front reaches 5; it is seen that the simulation (curves, in this case) models the experimental (symbols) ΔP_{4-5} quite well as both a function of volumetric flow rate (Q) and barrel-temperature setting (T_B) for both polystyrene (PS) and polypropylene (PP). Similar results have also been obtained with a polycarbonate. On the other hand, Fig. 3 compares corresponding experimental (symbols) and predicted (curves) gate pressure losses, from which it is

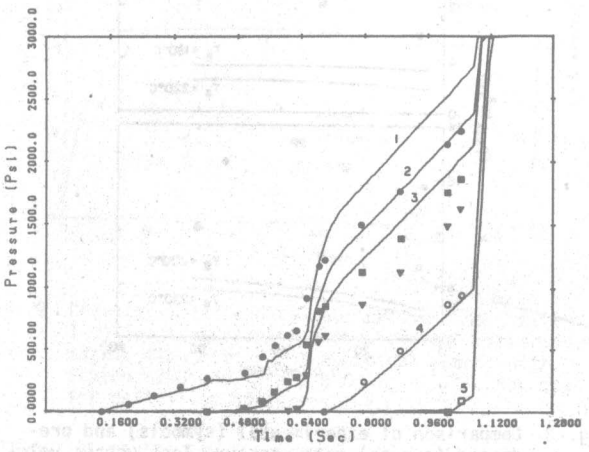

Fig. 1 Comparison of experimental (curves) and predicted (symbols) pressure traces during filling stage for polypropylene with T_B = 230°C, injection speed of 25% and T_W = 32°C.

seen that the measured values are almost four times as large in some instances. Noting that the gate in the present case corresponds to a rectangular slit with half-gap thickness (b) of .05 cm, width (W) of .6 cm and length (L) of .5 cm, such that L/b = 10, it follows that the extra pressure loss in Fig. 3 can be interpreted in terms of an extra equivalent length (L_e) of the gate. It then follows that $L_e/b \simeq 27$ (27) for PS at 180°C (220°C) and $\simeq$ 30 (15) for PP at 200°C (230°C). Similar results for polycarbonate indicate a much smaller effect, with $L_e/b \simeq 8$ at 330°C.

As another means of studying juncture pressure losses, experiments have been performed using a laboratory screw extruder attached to a die consisting of a cylindrical reservoir and an interchangeable capillary. By measuring the pressure drop versus flow rate for

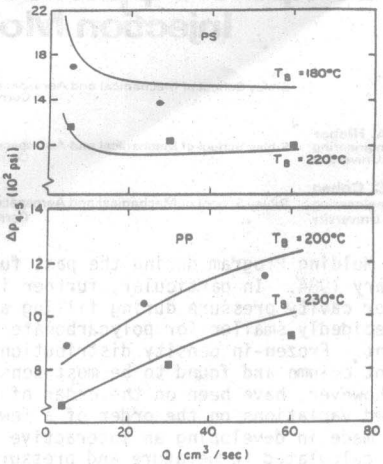

Fig. 2 Comparison of experimental (symbols) and predicted (curves) results for cavity-pressure difference ΔP_{4-5} versus volumetric flow rate for polystyrene and polypropylene at various barrel temperatures.

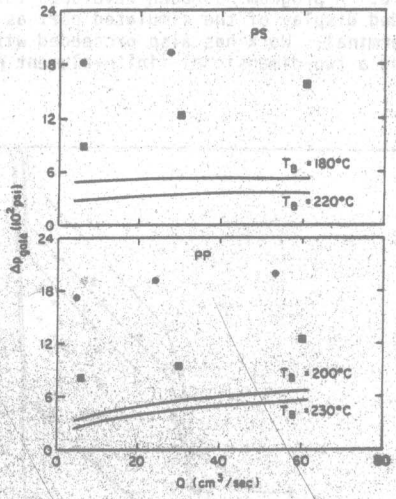

Fig. 3 Comparison of experimental (symbols) and predicted (curves) gate-pressure loss versus volumetric flow rate for polystyrene and polypropylene at various barrel temperatures.

different lengthed capillaries (corresponding to length-to-diameter ratios of .45, .77, 1.33, 3.33, 6.67 and 13.3), it has been possible to extrapolate the pressure drop to a capillary of zero length and thereby determine the effective juncture loss. When expressed in terms of an extra equivalent length, the experimental results are as shown in Figs. 4 and 5 where R denotes the capillary radius and $\dot{\gamma}_w$ is the shear rate at the capillary wall under fully-developed flow. As in the previous experiments, it is seen that the values of L_e are comparable for polystyrene (PS) and polypropylene (PP) but substantially smaller for polycarbonate (PC); further, the presence of glass-fiber fillers is seen to appreciably increase the juncture loss.

In a related area, work has continued with the measurement of flow birefringence and pressure losses for two-dimensional channel flows, as indicated in Fig. 6, with the flow directed either upwards (diverging flow) or downwards (converging flow). The polymeric

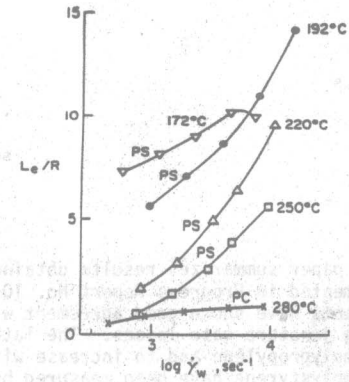

Fig. 4 Dependence of non-dimensional extra length, L_e/R, versus $\dot{\gamma}_w$ for PS Styron 678U at various temperatures and for PC Lexan 141-112 at 280°C.

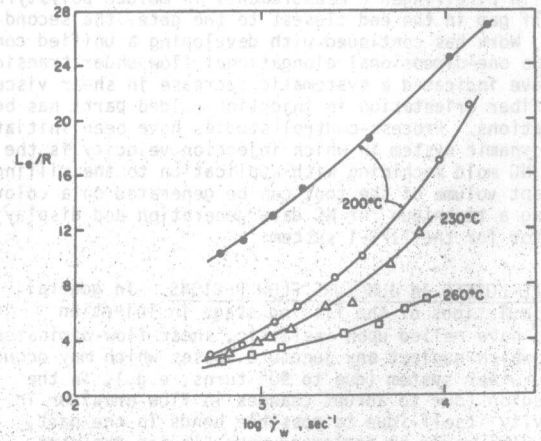

Fig. 5 Non-dimensional extra length, L_e/R, versus shear rate for pure PP melt (open symbols) at different temperatures and for 40% glass-fiber-filled PP melt (solid) at 200°C.

material in this case is polyisobutylene, which remains molten at room temperature. Typical results are shown in Figs. 7 and 8. In particular, it is noted that, for the same flow rate, the birefringence level is higher in converging flow even though the pressure loss is higher in diverging flow. As a point of reference, it might be noted that inelastic modelling would give the same results for both converging and diverging flow. Accordingly, the differences between curves 1 and 2 in Figs. 7 and 8 must be addressed in terms of viscoelastic modelling, an area in which we are continuing investigation.

PRESSURE LOSSES IN NON-CIRCULAR RUNNERS. A further complication in injection molding concerns the flow of polymeric melts in non-circular (typically trapezoidal or half-round) runners under non-isothermal conditions. In this regard, we have performed runner experiments corresponding to the extrusion of polymeric melt through an open-ended, non-circular, cold-wall die. Typical results are shown in Fig. 9 which plots the measured (circles) steady-state overall pressure drop along a trapezoidal runner for a commercial polystyrene together with corresponding predictions (curves) based upon various models. In particular, curves I and II correspond to a model in which the dependence of the shear viscosity (η) upon shear rate ($\dot{\gamma}$) and temperature (T) is assumed to be of the form:

$$\eta(\dot{\gamma},T) = \frac{\eta_o(T)}{1 + C(\eta_o\dot{\gamma})^{1-n}} \quad , \quad \eta_o(T) = B\exp(T_b/T) \qquad (1)$$

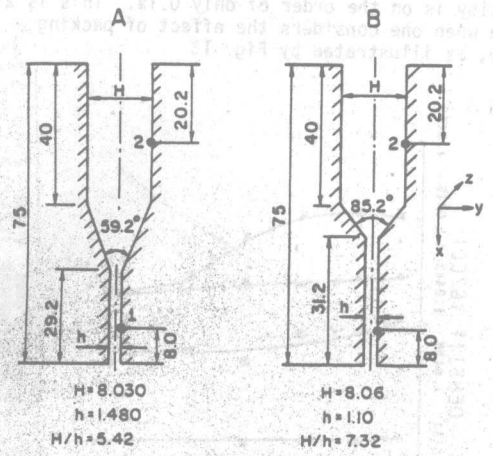

Fig. 6 Diagram for working cells A and B. Points 1 and 2 indicate the locations of flush-mounted pressure transducers. All dimensions in mm.

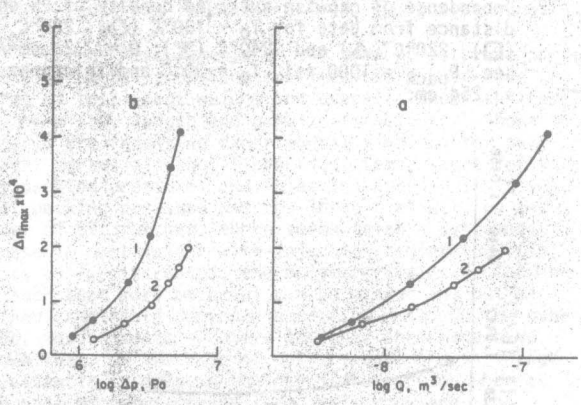

Fig. 7 Maximum of birefringence along centerline versus volumetric flow rate (a) and pressure drop (b) for converging (curve 1) and diverging (curve 2) flow. Data for working cell B in Fig. 6.

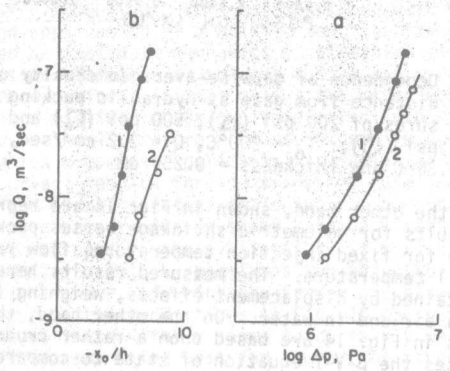

Fig. 8 (a) Pressure drop versus volumetric flow rate for converging (curve 1) and diverging (curve 2) flow. (b) Channel length, x_0/h, at which centerline birefringence starts to build up in converging flow (curve 1), or completely relaxes in diverging flow (curve 2), versus volumetric flow rate. Data for working cell B in Fig. 6.

where $\eta_0(T)$ denotes the zero-shear-rate (newtonian) viscosity and n, T_b, B and C are constants for given material. The difference between I and II is due to the fact that I replaces the actual runner with an equivalent circular runner of the same hydraulic radius (and scales the flow rate down such that the same average velocity is maintained as in the actual runner) whereas II takes the equivalent circular runner to have the same flow area as the actual. Of the two, it is seen that the former procedure describes the data much better. It is noted further that curve III is the same as I except for replacing Eqn. (1) by its power-law limit for large $\dot{\gamma}$. Accordingly, the closeness of I and III indicates that the power-law approximation would be adequate under the present flow conditions with polystyrene. Such has not been the case, however, with corresponding results with polycarbonate. In addition, it is noted that curve IV in Fig. 9 is the same as I except that a pressure dependence has been incorporated into Eqn. (1) by adding a multiplicative factor $\exp(\beta p)$ to the expression defining η_0. Although the effect of this pressure dependence is not significant in the present case, where the pressures are only ≈ 2500 psi, the present results imply that this effect could be rather substantial in actual applications where pressures on the order of 10,000 psi are not unusual. Finally, curve V in Fig. 9 is the same as I except for the absence of non-isothermal effects, clearly indicating the inadequacy of isothermal modelling in the present situation. In particular, curve I lies above V at small flow rates due to conduction cooling to the cold wall whereas it lies below V at high flow rates due to viscous-heating effects.

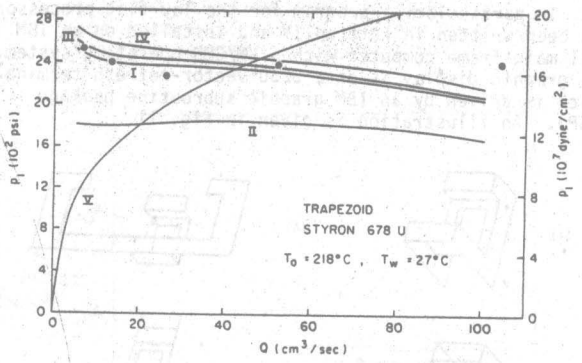

Fig. 9 Data (symbols) and various predictions (curves I-V) for steady-state pressure drop versus volumetric flow rate for trapezoidal runner with Styron 678U and T_0 = 218°C, T_w = 27°C. See text for definition of curves I-V.

INTERACTIVE CAVITY-FILLING PROGRAM. Work has proceeded with a proposed CAD system aimed at reducing the input/output requirements in applying our two-dimensional (finite-element/finite-difference) cavity-filling program. As indicated in Fig. 10, the system will consist of three parts: lay flat, mesh generation and display processors. The lay-flat processor will be used to unfold any three-dimensional thin part such that all surfaces lie in one plane. This procedure will simplify a 3-D flow-analysis problem into 2-D. The mesh-generation processor will assist the user in allocating the domain occupied by the polymer melt flow during each time interval, and allow the user to interactively define new elements within this domain. For each time step, new elements will be created and added to the input data of the flow-analysis program until the entire cavity gets filled. The display processor will interpret the numerical results for the pressure and temperature by means of color intensity such that the pressure and temperature distributions, gradients and contours can be easily "seen" on a color terminal. Another useful display will be a three-dimensional short-shot sequence representing the actual formation of an injection-molded part in the cavity and indicating the weld-line positions and

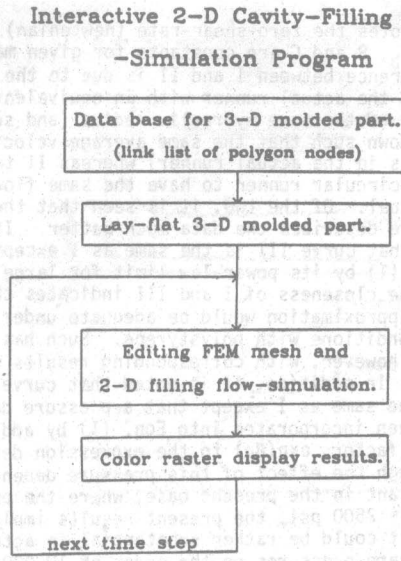

Fig. 10 Flowchart for interactive 2-D cavity-filling flow-simulation program.

desirable locations for venting. The proposed system will be directed towards providing an interface between the user and the numerical-analysis program such that the simulation can be easily applied to real problems.

In particular, a program for the lay-flat processor has been written in Fortran IV and installed on an IBM 4341 main-frame computer with a VM/CMS operating system. The graphic display is on a 3250 vector-refresh terminal which is driven by an IBM graphic subroutine package (GSP). An illustration is given in Fig. 11.

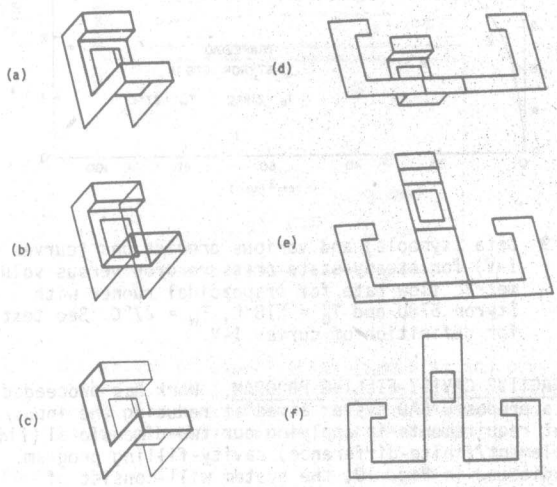

Fig. 11 Example of lay-flat sequence.

SHRINKAGE AND DENSITY VARIATIONS IN MOLDED PARTS. Density distributions in injection-molded samples of polystyrene have been carefully measured with a density-gradient column. Representative results are shown in Fig. 12 which plots the frozen-in gapwise-averaged density versus distance from gate (strip mold) for various injection temperatures, all for the same flow rate, packing pressure and mold wall temperature. In particular, it is noted that the parts made with a lower injection temperature have a lower final density. This is due to a larger non-equilibrium effect in such parts which arises from the fact that the relaxation time of polymer melts increases with decreasing temperature. It is noted further, however, that the overall variation in the density is on the order of only 0.1%. This is also the case when one considers the effect of packing pressure, as illustrated by Fig. 13

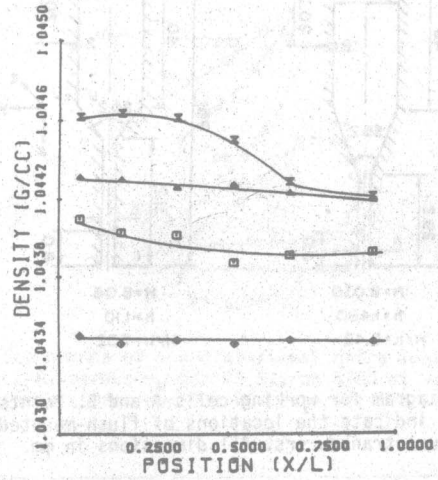

Fig. 12 Dependence of gapwise-averaged density of PS on distance from gate for T_o = 180°C (◇), 200°C (□), 220°C (△) and 240°C (⧗); Q = 7.2 cm^3/sec, P_{pack} = 1000 psi, T_w = 30°C and thickness = .254 cm.

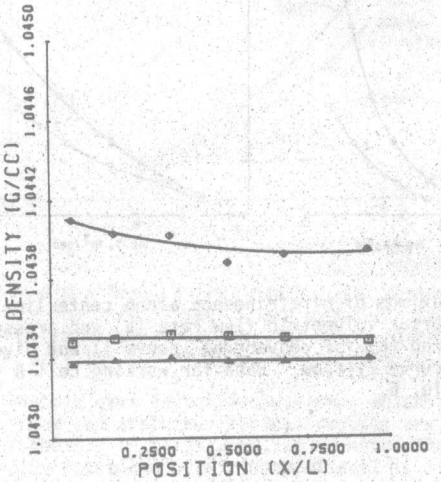

Fig. 13 Dependence of gapwise-averaged density of PS on distance from gate at hydraulic packing pressures of 200 psi (△), 500 psi (□) and 1000 psi (◇); T_o = 200°C, Q = 7.2 cm^3/sec, T_w = 30°C and thickness = 0.254 cm.

On the other hand, shown in Fig. 14 are representative results for volumetric shrinkage versus packing pressure for fixed injection temperature, flow rate and mold wall temperature. The measured results here have been obtained by displacement effects, weighing the parts in air and in water. On the other hand, the predictions in Fig. 14 are based upon a rather crude model which uses the p-V-T equation of state to compare a representative specific volume during the cooling stage (using experimental pressure traces for p and calculating T based upon transient one-dimensional conduction) with the corresponding specific volume under room temperature and atmospheric pressure. Despite the crudeness of the modelling, the predictions are seen to do fairly well concerning both the trend and the order-of-magnitude of the effect.

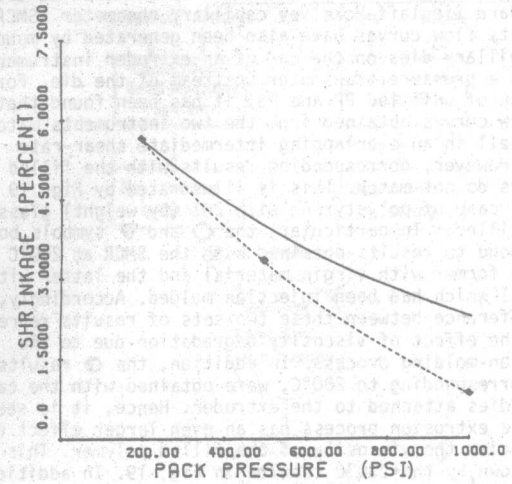

Fig. 14 Measured (◇) and predicted (solid line) total volumetric shrinkage vs. hydraulic packing pressure; T_0 = 220°C, Q = 72 cm^3/sec, T_W = 30°C and thickness = 0.254 cm; polystyrene.

Further measurements on the same polystyrene parts and also on polypropylene specimens have been made in terms of total part weight and overall linear shrinkage in the width, length and gapwise directions. Shown in Fig. 15 are resulting experimental findings for part weight versus air-shot (injection) temperature for various packing pressures and injection speeds. It is seen that packing pressure has the largest effect, on the order of 5%; further, there seems to be a systematic increase in part weight with injection temperature (in fact, as T_{as} increases, the polymer remains molten longer such that more material can be packed in) but a rather negligible dependence on flow rate. On the other hand, measurements of overall linear shrinkage have shown that, in the case of polystyrene, the shrinkage is essentially only in the gapwise direction whereas, in the case of (semi-crystalline) polypropylene, the shrinkage in the width and length directions are no longer negligible. In both cases, however, the sum of the three linear shrinkages, corresponding to the volumetric shrinkage, can account for the variations in part weight shown in Fig. 15. That is, part-weight variations are due essentially to changes in part dimensions rather than in part density.

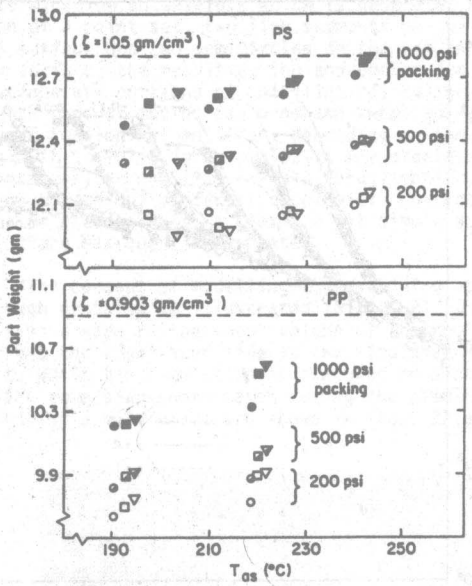

Fig. 15 Part weight versus air-shot temperature for various hydraulic packing pressures {solid (1000 psi), half solid (500 psi), open (200 psi)} and injection speeds {circle (7.2 cm^3/sec), square (36 cm^3/sec), triangle (72 cm^3/sec)} for polystyrene and polypropylene.

VISCOELASTIC MODELLING. Work has continued with development and application of a unified constitutive equation based on continuum mechanics supplemented with consideration of molecular network theory and irreversible thermodynamics. In particular, the model equation has now been applied to various rheological experiments available in the literature. One such case is shown in Fig. 16 which compares experimental (symbols) and predicted (curves) results for the transient development of shear and normal stresses following the abrupt imposition of a steady uniform shear rate of 1 sec^{-1}. It is noted that, pending the availability of more extensive rheological data, the model has two adjustable parameters, a and r, of which the former has essentially no effect on the predictions in Fig. 16 whereas the range between 1 and 4 for r seems to do fairly well, with $r \approx 2$ perhaps being best for the normal stresses and $r \approx 4$ for the shear stress. Further comparisons for the same low-density polyethylene melt are shown in Fig. 17 for the transient elongational viscosity following the abrupt imposition of a steady uniform elongational strain rate of magnitude $\dot{\epsilon}$ (sec^{-1}). In particular, the lower bound ($\dot{\epsilon}$ = .001 sec^{-1}) in Fig. 17 corresponds to linear viscoelasticity. As in Fig. 16, the predictions are again essentially independent of a. It is seen that the comparison with data improves at the larger values of r in Fig. 17. Similar reasonable agreement has been obtained with corresponding

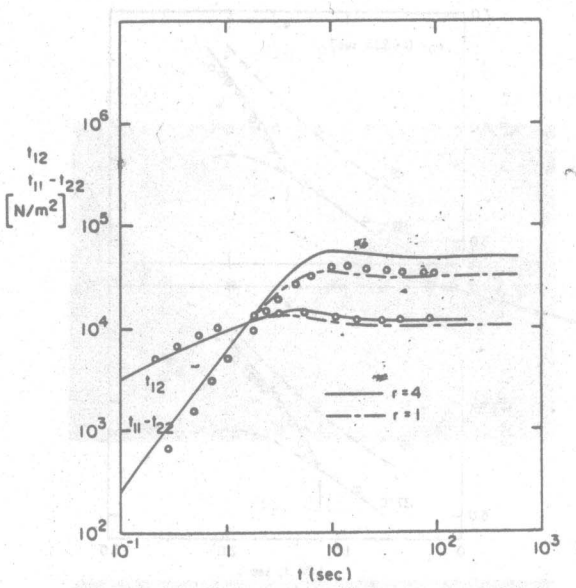

Fig. 16 Shear stress t_{12} and first-normal-stress difference $t_{11} - t_{22}$ as functions of time (r = 4 or 1 and a = 1) at $\dot{\gamma}$ = 1 sec^{-1}. Symbols: experimental data for low-density polyethylene at 150°C by Laun (1978).

experimental results involving polypropylene, polystyrene and polyisobutylene.

In extending viscoelastic modelling to non-isothermal situations, as occur in injection molding, the Leonov constitutive equation has been applied to transient elongational flow experiments in which the temperature undergoes prescribed temporal variations. Such non-isothermal effects are handled by incorporating a temperature dependence of the model parameters based upon the well-known WLF equation. Shown in Fig. 18 are typical

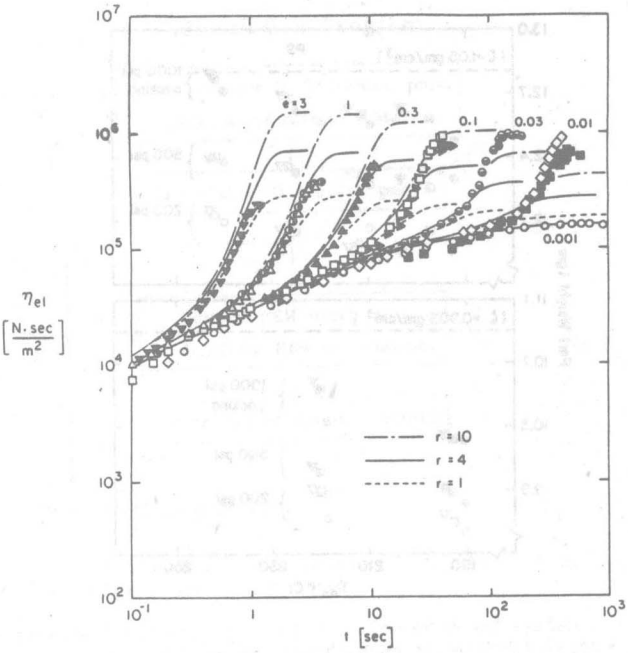

Fig. 17 Elongational viscosity as a function of time at several elongational rates for low-density polyethylene at 150°C; filled symbols: data from Munstedt and Laun (1979); blank symbols: data from Meissner (1972).

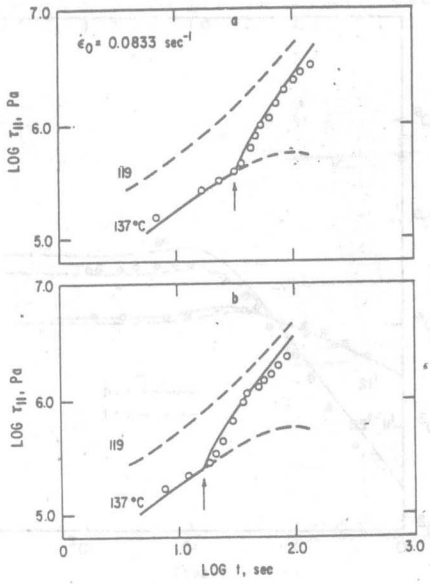

Fig. 18 Tensile stress τ_{11} as a function of time under constant pulling speed (an initial strain rate of 0.0833 s^{-1}). Temperature drops from 137°C to 119°C at times indicated by arrows in (a) and (b).

comparisons between data (symbols) and predictions (curves) for a commercial-grade polystyrene which is abruptly subjected to a constant pulling speed at t = 0 (the elongational strain rate therefore decreasing monotonically from its initial value, $\dot{\epsilon}_0$) and then subjected to an abrupt change in its temperature at some later time. The agreement is seen to be quite reasonable in both cases shown in Fig. 18, as it has been found in many other cases also.

GLASS-FIBER-FILLED THERMOPLASTICS. In addition to using a standard Sieglaff-McKelvey capillary rheometer (SMCR), viscosity flow curves have also been generated by mounting capillary dies on the end of an extruder instrumented with a pressure transducer upstream of the die. For the case of unfilled PP and PS, it has been found that the flow curves obtained from the two instruments match quite well in an overlapping intermediate shear-rate range. However, corresponding results with the filled polymers do not match. This is illustrated by Fig. 19 for the case of polystyrene with 20% (by weight) glass-fiber filler. In particular, the ◇ and ▽ symbols both correspond to results obtained with the SMCR at 200°C but the former with virgin material and the latter with material which had been injection molded. Accordingly, the difference between these two sets of results represents the effect of viscosity degradation due to the injection-molding process. In addition, the ◑ results, also corresponding to 200°C, were obtained with the capillary dies attached to the extruder. Hence, it is seen that the extrusion process has an even larger effect upon reducing the viscosity of the filled polymer. This is also shown by the 230°C results in Fig. 19. In addition, as a further check, the △ results in Fig. 19 correspond to measurements on the SMCR with material which had been extruded. The fact that these results merge with the ▽ indicates the self-consistency of the present results and also shows that the SMCR does not itself alter the viscosity of the filled polymer. These findings therefore indicate that, for the purpose of simulating the injection molding of filled thermoplastics, the viscosity flow curves should be generated with material which has been first injection molded.

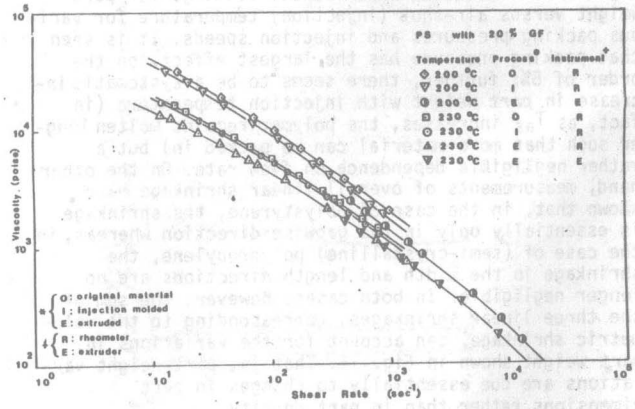

Fig. 19 Processing effects on the viscosity curves of polystyrene with 20% glass-fiber filler.

MOLD MACHINING. An experimental system has been developed for the simulation of NC mold machining with application to the milling operation. Based on set theory, a simulated machined part can be modelled by subtracting (Boolean difference) the swept volume of the tool motion from the workpiece. The shaded display of the simulated machined part as well as the swept volume of the tool can be generated on a color-raster graphic terminal.

. The shape of the workpiece can be modelled by any existing solid geometric modelling system which is capable of providing the "ray casting" information of the modelled object for generating the shaded image. Essentially, the information is obtained by tracing light rays from the observing point to the object. The coordinates of the entry and exit points are found by determining the intersections of the ray (a line) and the boundary faces of the object. The first intersecting point is visible and thus retained for the purpose of shading the image of the object. All intersections must be used if the Boolean subtraction of the swept volume is to be performed.